Efficient Recycling of Dilute Nitrate to Ammonia using Cu Nanowire Electrocatalyst

Kaige Shi,[1] Maia D. Willis,[2] Zhuanghe Ren,[1] and Xiaofeng Feng[1,2,3,4]*

[1]Department of Physics, University of Central Florida, Orlando, Florida 32816, United States

[2]Department of Chemistry, University of Central Florida, Orlando, Florida 32816, United States

[3]Renewable Energy and Chemical Transformations (REACT) Cluster, University of Central Florida, Orlando, Florida 32816, United States

[4]Department of Materials Science and Engineering, University of Central Florida, Orlando, Florida 32816, United States

*Email: Xiaofeng.Feng@ucf.edu (X.F.)

ABSTRACT:

Electrochemical reduction of nitrate provides a sustainable route for the recycling of waste nitrate to valuable ammonia when powered by electricity from renewable sources. Development of such a process requires efficient electrocatalysts than can facilitate high single-pass conversion of dilute nitrate to ammonia. Here we report a Cu nanowire electrocatalyst for nitrate reduction, which was prepared by growing Cu nanowires with tunable morphology and density on a Cu foam substrate. Compared to the Cu foam, the Cu nanowires created new catalytic sites and greatly enhanced the activity and selectivity for nitrate reduction to ammonia. As a result, the optimized Cu nanowire electrode showed a 3-fold increase of the nitrate reduction activity with a 90% Faradaic efficiency for ammonia production at a low overpotential of −0.1 V vs RHE in an electrolyte containing 5 mM nitrate, which is attributed to the high catalytic surface area with an appropriate combination of Cu(100) and Cu(111) facets. The electrode was further tested for continuous nitrate electrolysis using a flow cell, which achieved a 76% single-pass conversion of nitrate with a 93% ammonia Faradaic efficiency, demonstrating a great promise for applications in wastewater treatment and sustainable ammonia synthesis.

INTRODUCTION

Electrocatalysis plays a central role in the development of renewable energy technologies to mitigate the global energy and environmental problems, such as the nitrate (NO_3^-) contamination of water resources caused by the increasing use of nitrogen fertilizers as well as the discharge of industrial wastewater.[1] The use of nitrogen fertilizers has contributed significantly to the growth of agricultural production, but the nitrogen use efficiency is typically lower than 40%,[2] so that a significant amount of nitrogen readily leaches into groundwater, lakes, and rivers, increasing the concentration of NO_3^- in the water systems and causing severe environmental problems such as eutrophication.[3,4] It is thus urgent to develop technologies that can efficiently remove NO_3^- from wastewater, preferably using energy from renewable sources. Among the various strategies, the electrochemical reduction of NO_3^- to ammonia (NH_3) has recently emerged as a promising route as it is compatible with the intermittent supply of solar- or wind-generated electricity to enable a sustainable process for the recycling of NO_3^- as well as the production of NH_3 as an alternative to the Haber−Bosch process.[5−7]

Development of a NO_3^- recycling process requires electrocatalysts with a high activity and selectivity for NO_3^- reduction to NH_3.[8−10] This is however challenging due to the various products of the NO_3^- reduction reaction (NO_3RR) as well as the competition of the hydrogen evolution reaction (HER). In addition to the desired product NH_3, the electroreduction of NO_3^- also forms other side products such as NO_2^- and N_2,[8] thus compromising the selectivity for NH_3 production. Moreover, when a relatively high overpotential is applied, the HER may become competitive and further lower the Faradaic efficiency of the NO_3RR. Therefore, studies have focused on catalytic materials that are relatively inert for the HER, such as Cu-, Co-, Ti-, and carbon-based materials, and single-atom catalysts.[11−21] In particular, Cu shows a high activity for the NO_3RR,[22] so that various Cu-based nanostructures, heterostructures, and alloys have been developed to enhance the NO_3RR activity and selectivity,[23−35] such as Cu-Ni alloys,[26] Cu nanosheets,[28] oxide-derived Cu,[30] and Ru-dispersed Cu nanowires.[32] Despite the substantial progress, development of an efficient NO_3^- recycling process further requires electrodes with a high single-pass conversion of dilute NO_3^- to NH_3 to demonstrate the practical viability for wastewater treatment, considering the low concentration of NO_3^- in typical wastewater sources (e.g., a few mM).[3,4]

Here, we present a study of Cu nanowire electrocatalysts for the electroreduction of NO_3^- to NH_3 with high activity and selectivity. We prepare a series of Cu nanowire samples with tunable morphology and density by immersing Cu foams in the alkaline ammonium persulfate solution to form $Cu(OH)_2$ nanowires, followed by annealing and electrochemical reduction to obtain metallic Cu nanowires. Compared to the Cu foam, the Cu nanowire electrodes show generally improved electrocatalytic performance for the NO_3RR, achieving a current density of 20.8 mA cm^{-2} and a NH_3 Faradaic efficiency of 90% on an optimized electrode at −0.1 V vs the reversible hydrogen

electrode (RHE) in an electrolyte with dilute NO_3^- (5 mM). Moreover, the Cu nanowire electrode is further tested for continuous NO_3^- recycling using a flow cell, which reaches a 76% single-pass conversion of dilute NO_3^- to NH_3 while maintaining a NH_3 Faradaic efficiency of 93%. Our work demonstrates a promising method for an efficient recycling of low-concentration NO_3^- to valuable NH_3 using facilely fabricated Cu nanowire electrodes.

EXPERIMENTAL METHODS

Preparation of Cu foam samples. Typically, commercial Cu foam samples of 0.5 × 0.5 cm^2 were first washed with isopropanol and then 0.05 M H_2SO_4 solution to clean the surface,[32] followed by rinsing with deionized water and drying under a stream of Ar gas. The as-prepared samples are referred to as Cu foam samples.

Preparation of Cu nanowire samples. The Cu nanowire samples were prepared as follows: a pre-cleaned Cu foam was soaked in a solution containing 0.067 M $(NH_4)_2S_2O_8$ and 1.333 M NaOH at ambient conditions for various time intervals (0−20 min) to form $Cu(OH)_2$ nanowires.[36] The synthesized $Cu(OH)_2$ nanowire sample was rinsed with deionized water and dried under a stream of Ar gas. After that, the $Cu(OH)_2$ nanowire sample was annealed in air at 150°C for 2 h to obtain CuO nanowire sample,[37] which was then assembled into an H-cell and electrochemically reduced by cyclic voltammetry (CV) scans from 0.25 to −0.45 V vs RHE in 1 M KOH electrolyte at a scan rate of 100 mV s^{-1} for 5 cycles to derive a Cu nanowire sample.

Characterizations. Scanning electron microscopy (SEM) images were acquired using a ZEISS Ultra-55 FEG scanning electron microscope. Grazing-incidence X-ray diffraction (XRD) patterns were collected using a PANalytical Empyrean diffractometer with an incidence angle of 5°. X-ray photoelectron spectra (XPS) were obtained using a Thermo Scientific ESCALAB XI^+ X-ray photoelectron spectrometer with an Al Kα X-ray source (1486.67 eV).

Electrochemical measurements. All electrochemical measurements were mainly performed using a Gamry Interface 1000 potentiostat and a gas-tight two-compartment electrochemical cell (H-cell) separated using a piece of Fumasep FAA-3-PK-130 anion exchange membrane at room temperature, as schematically shown in Figure S1. In the H-cell experiments, a piece of Pt gauze and a Hg/HgO electrode (filled with 1 M KOH solution) were used as the counter electrode and reference electrode, respectively. The anion exchange membranes were first rinsed with water and immersed in 0.5 M NaCl solution for at least 72 h, then immersed in 1 M KOH solution for at least 24 h and rinsed with water before use. In addition, single-pass conversion tests were performed using a Gamry Interface 1000 potentiostat and a home-built flow cell, in which a piece of Fe−Ni foam and a leak-free Ag/AgCl electrode were used as the counter electrode and reference electrode, respectively. The electrochemical reduction of nitrate was tested by both linear sweep voltammetry (LSV) and bulk electrolysis in 1 M KOH electrolytes containing various concentrations of NO_3^-

(1−50 mM). Prior to an electrolysis, the catholyte was bubbled by Ar gas for 30 min to remove oxygen. During an electrolysis, the catholyte was stirred at a rate of 600 rpm with Ar gas purging at 5 sccm. In addition, 0.05 M H_2SO_4 solution was used as an in-line acid trap to capture ammonia that might possibly escape from the catholyte, as illustrated in Figure S1. All potentials were iR-compensated and converted to the RHE scale in this study. The reported current densities were normalized to the geometric surface areas of electrodes. Gas-phase product of the NO_3^- reduction electrolysis was quantified by periodic gas chromatography (GC) of the H-cell headspace. The produced NH_3 in the catholyte was quantified by the indophenol blue method,[38] based on the calibration curve in Figure S2. The produced NO_2^- in the catholyte was quantified by the Griess method,[39] based on the calibration curve in Figure S3. Possible NH_3 in the acid trap was also quantified by the indophenol blue method. In addition, ^{15}N isotopic labeling experiment was performed with $^{15}NO_3^-$ reactant to verify the N source of the detected NH_3 using nuclear magnetic resonance (NMR) spectroscopy (calibration curve in Figure S4).

Quantification of ammonia. The concentration of produced ammonia in the electrolyte was quantified using indophenol blue method.[38] The calibration curves were established from standard NH_4Cl solution of different concentrations (0−0.10 mM) in a background solution. Typically, 5 mL of the standard NH_4Cl solution was pipetted into a precleaned vial. Then, 2 mL of 1 M NaOH solution containing salicylic acid (5 wt%) and sodium citrate (5 wt%) was added, and subsequently 1 mL of NaClO solution (0.05 M) and 0.2 mL of sodium nitroferricyanide solution (1 wt%) were added. After 2 h, UV-visible absorption spectra of the solution were acquired using a Thermo Scientific Evolution 201 UV-Vis Spectrophotometer. The formed indophenol blue was measured by the absorbance at λ = 655 nm. The produced NH_3 in the catholyte was quantified using the same procedure but with the catholyte, which was diluted with the same background solution (such as 1 M KOH, so that the pH of the test solution remained the same) to ensure that the concentration of ammonia in the test solution was in the linear range of the indophenol blue method (Figure S2).

Quantification of nitrite. The concentration of produced nitrite (NO_2^-) in the electrolyte was quantified by the Griess method.[39] A mixture of p-aminobenzenesulfonamide (4 g), N-(1-Naphthyl) ethylenediamine dihydrochloride (0.2 g), phosphoric acid (10 mL, ρ = 1.70 g/mL), and deionized water (50 mL) was used as a color reagent. Typically, a certain amount of the electrolyte was taken out from the cell and diluted to ensure that the nitrate concentration in the test solution was in the linear range of the Griess method. Then, 0.1 mL of the color reagent was added to the solution and mixed. After 20 min, UV-visible absorption spectra of the solution were acquired using a Thermo Scientific Evolution 201 UV-Vis Spectrophotometer, and the absorbance at λ = 540 nm was used to quantify the concentration of nitrate, based on the calibration curve in Figure S3.

Calculation of nitrate reduction Faradaic efficiency. The Faradaic efficiencies for NH_3 and NO_2^- production in the NO_3^- reduction electrolysis were calculated from the charge consumed for NH_3 and NO_2^- production and the total charge passing through the electrode:

$$\text{Faradaic efficiency } (NH_3) = (8F \times c_{NH_3} \times V \times \text{diluted times})/Q$$

$$\text{Faradaic efficiency } (NO_2^-) = (2F \times c_{NO_2^-} \times V \times \text{diluted times})/Q$$

where F is the Faraday constant, c_{NH_3} and $c_{NO_2^-}$ are the molar concentrations of NH_3 and NO_2^- measured in the diluted catholyte, respectively, V is the volume of the catholyte, and Q is the total charges passing through the electrode during the electrolysis.

^{15}N isotope labeling experiment. The ^{15}N isotope labeling experiment was carried out using 1 M KOH + 5 mM $K^{15}NO_3$ (98 atom % ^{15}N) solution as the electrolyte. The post-reaction catholyte was acidized to pH ~3 by adding H_2SO_4 solution. Afterward, 900 μL of the acidized catholyte was mixed with 100 μL of D_2O containing 100 ppm dimethyl sulfoxide (DMSO) as an internal standard. The $^{15}NH_4^+$ was detected by ^1H NMR spectroscopy using a Bruker AVANCE III 500 MHz.

Measurement of electrochemical surface area (ECSA). The ECSA of a Cu foam or Cu nanowire electrode is proportional to its double-layer capacitance, which was measured by a CV method. CV scans were performed on an electrode at different scan rates ranging from 10 to 100 mV s^{-1} in the potential window of −0.1 to 0 V vs RHE, where only double-layer charging and discharging occur. The double-layer charging current was then derived and plotted against the CV scan rate, and the slope of the linear regression gives the double-layer capacitance of the electrode.

RESULTS AND DISCUSSION

To develop efficient electrocatalysts for the NO_3RR, we started with commercial Cu foam as a substrate and grew Cu nanowires on it to create new catalytic sites. The Cu nanowire samples were prepared by soaking a pre-cleaned Cu foam in a solution containing 0.067 M $(NH_4)_2S_2O_8$ and 1.333 M NaOH at ambient conditions for various time intervals (0−20 min) to form $Cu(OH)_2$ nanowires,[36] which were then annealed in air at 150°C for 2 h to obtain CuO nanowires[37] and further electrochemically reduced to derive Cu nanowires (see the Experimental Methods in the Supporting Information for details). A series of Cu nanowire samples were prepared in this way by adjusting the soaking time of Cu foam in the solution (2, 6, 10, 15, and 20 min), thus to tune the morphology and density of the derived nanowires. The prepared samples are hereafter referred to as CuNW-2, CuNW-6, CuNW-10, CuNW-15, and CuNW-20 electrodes, respectively. SEM images were acquired to visualize the morphologies of the Cu foam and Cu nanowire samples, are shown in Figure 1 with larger-scale SEM images in Figure S5. The surface morphology of the Cu foam was largely smooth at the micrometer scale (Figure 1a), while Cu nanowires were clearly

visible on the nanowire samples (Figure 1b−f). Along with the increase of the soaking time, the derived nanowires became longer, thicker, and denser, and entangled to form bundles in the CuNW-10, CuNW-15, and CuNW-20 samples. Such a series of samples allow us to study the effect of electrode morphology and nanostructure in the NO_3RR.

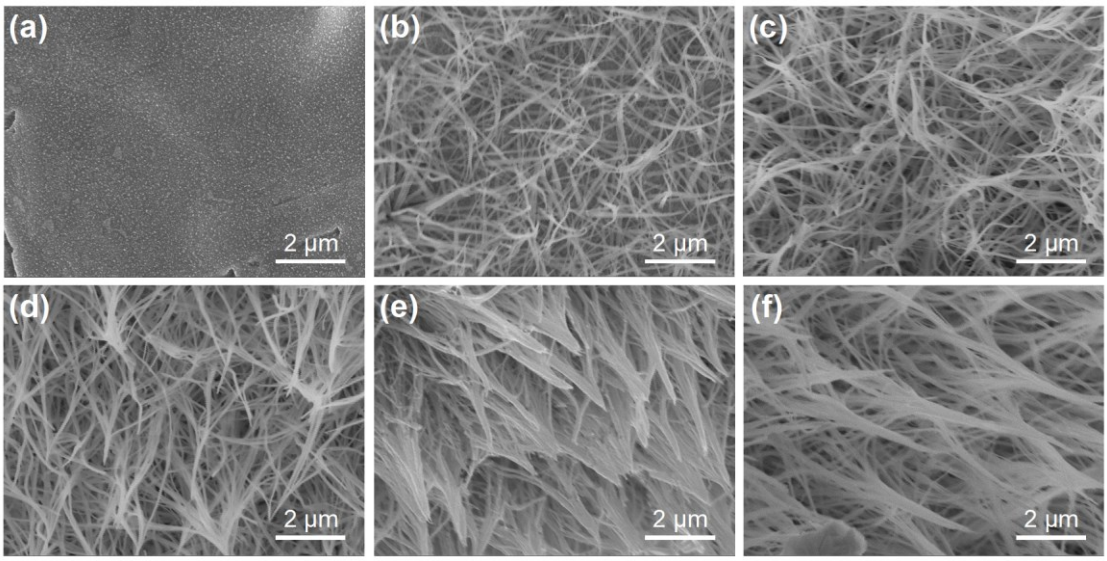

Figure 1. SEM images of the as-prepared Cu foam and Cu nanowire electrodes: (a) Cu foam; (b) CuNW-2; (c) CuNW-6; (d) CuNW-10; (e) CuNW-15; and (f) CuNW-20.

The samples were further characterized by XRD and XPS to examine the crystalline structure and chemical state. For conciseness, here the CuNW-15 sample was selected as a representative Cu nanowire sample. As shown in Figure 2a, the grazing-incidence XRD patterns of the surface layer of the Cu foam and CuNW-15 samples both showed the (111), (200), and (220) diffraction peaks of metallic Cu in face-centered cubic structure. The XPS survey spectra of the Cu foam and CuNW-15 samples are presented in Figure S6, where only Cu and a small amount of O and C were identified on the two samples. As shown in Figure 2b, the two XPS peaks centered at ~932.3 and 952.2 eV were observed in the Cu 2p region,[40] and the fittings of the Cu 2p XPS spectra indicated that both Cu foam and CuNW-15 samples were predominantly metallic Cu. The Cu LMM Auger peaks were also used to examine the oxidation states of Cu.[41] As shown in Figure 2c, the Cu^0 LMM Auger peak at 568.2 eV was the major peak observed on the two samples, so they were mainly metallic Cu with a small amount of surface oxide due to air exposure, consistent with the Cu 2p XPS spectra in Figure 2b. Therefore, the XRD and XPS characterizations confirmed the metallic state of Cu on the foam and nanowire samples.

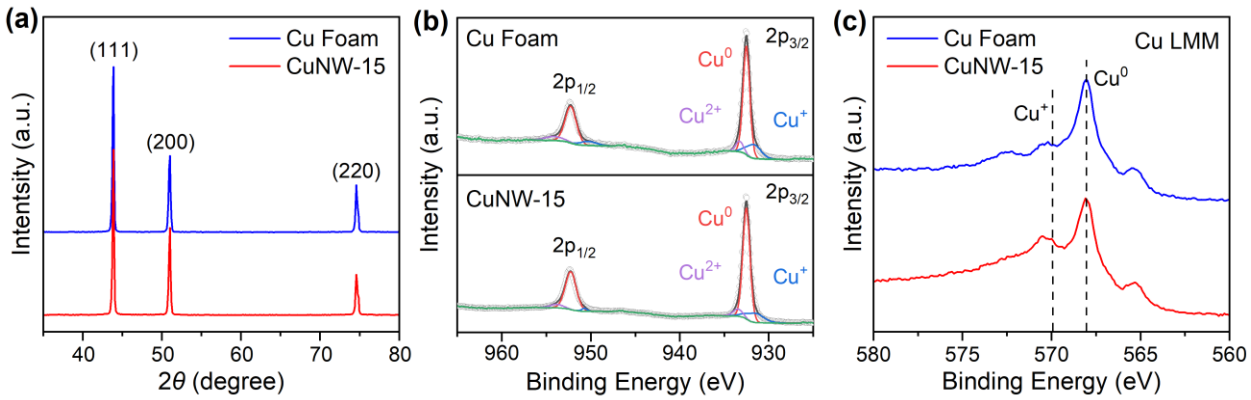

Figure 2. Characterization of the Cu foam and the CuNW-15 samples. (a) Grazing-incidence XRD patterns of the two samples. (b) Cu 2p XPS spectra of the two samples, with deconvoluted peaks fitted using the Gaussian fitting method. (c) Cu LMM Auger peaks of the two samples.

The Cu foam and Cu nanowire electrodes were then evaluated for the NO_3RR in a gas-tight two-compartment electrochemical cell (H-cell) with 1 M KOH electrolyte containing 5 mM KNO_3, as schematically shown in Figure S1. Particularly, a low concentration of NO_3^- was used in the electrolyte based on typical conditions of wastewater sources.[3,4] Linear sweep voltammetry (LSV) curves were recorded on the Cu foam, CuNW-2, CuNW-6, CuNW-10, CuNW-15, and CuNW-20 electrodes in the 1 M KOH + 5 mM KNO_3 electrolyte to evaluate the NO_3RR electrokinetics. As shown in Figure 3a, all current densities increased rapidly as the potential was swept from 0.2 to −0.3 V vs RHE (all potentials are reported with respect to this reference in this work). Compared to the Cu foam, the current densities on the Cu nanowire samples were generally higher in this potential range, indicating their improved activities for the NO_3RR. Along with the increase of the nanowire growth time, the current density increased monotonically from CuNW-2 to CuNW-15, which should be attributed to the morphology and catalytic surface of the Cu nanowires. The current density remained largely similar from CuNW-15 to CuNW-20, indicating that even longer growth of Cu nanowires beyond CuNW-15 did not further increase the NO_3RR activity in this case. In addition, the current densities on the Cu nanowire electrodes reached a plateau at around −0.2 V, which might be caused by the mass transport limitation of NO_3^- due to its low concentration. When the potential was swept to more negative than −0.25 V, the current density continued to increase rapidly, which was attributed to the rising of the HER activity.

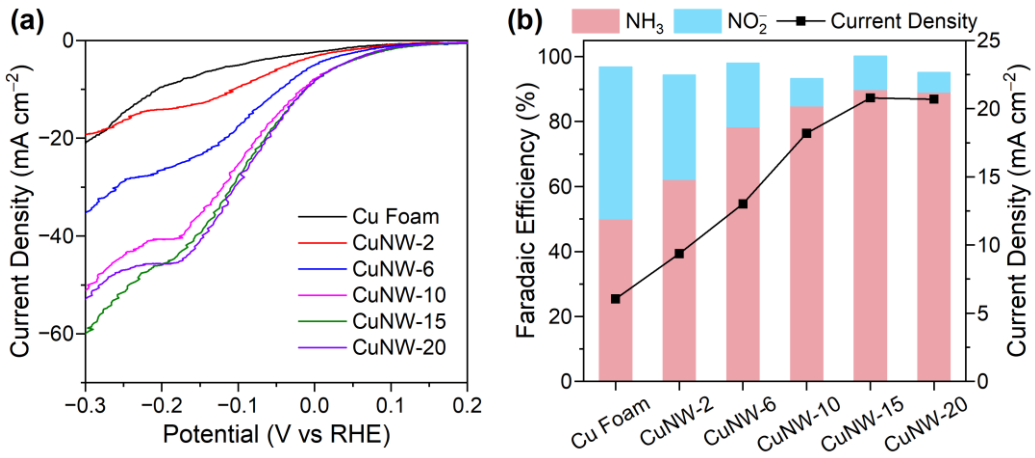

Figure 3. Evaluation of the NO_3RR performance on the Cu foam and Cu nanowire electrodes in H-cell. (a) LSV curves recorded on the Cu foam and Cu nanowire electrodes in 1 M KOH + 5 mM KNO_3 electrolyte. Scan rate: 10 mV s^{-1}. (b) Current densities and Faradaic efficiencies for the NO_3RR on the different electrodes, which were determined by bulk electrolysis at −0.1 V vs RHE for 30 min.

To quantify the NO_3RR product selectivity, bulk electrolysis was performed in H-cell with 1 M KOH + 5 mM KNO_3 electrolyte at −0.1 V vs RHE. This potential was selected as it can reflect the NO_3RR kinetics that were not limited by the mass transport or the HER competition yet. The representative chronoamperometric curves measured on the electrodes are exhibited in Figure S7, in which the current density decreased gradually with time: the higher the initial current density, the faster the decrease. This is attributed to the faster consumption of NO_3^- in the catholyte with a higher current density, so a moderate electrolysis time of 30 min was used to evaluate the NO_3RR performance. Two major products, NH_3 and NO_2^-, were detected in the catholyte and quantified by the indophenol blue method[38] and the Griess method,[39] respectively, based on the calibration curves in Figures S2 and S3. Furthermore, the N source of the detected NH_3 was confirmed to be the NO_3^- in the electrolyte using ^{15}N isotopic labeling experiment with NMR spectroscopy (calibration curve in Figure S4).

As shown in Figure 3b, the current density and NH_3 Faradaic efficiency were generally higher on the Cu nanowire electrodes than that on the Cu foam. As the nanowire growth time increased from 0 (Cu foam) to 15 min (CuNW-15), the current density increased by around 3-fold from 6.1 to 20.8 mA cm^{-2}, and the Faradaic efficiency for NH_3 production also increased monotonically from 50.1% to 90%. The CuNW-20 electrode showed a current density of 20.7 mA cm^{-2} with a NH_3 Faradaic efficiency of 89.2%, which were similar to that of the CuNW-15. Thus, the NO_3RR performance reached a plateau on CuNW-20 and did not further increase with the nanowire growth time, likely due to the mass transport limitation considering the low concentration of NO_3^- in the

electrolyte. Meanwhile, the Faradaic efficiency for NO_2^- production showed the opposite trend, decreasing from 46.6% (Cu foam) to 5.9% (CuNW-20), so the Cu nanowires greatly enhanced the selective conversion of NO_3^- to NH_3 while suppressing the production of NO_2^-. To explain the different NO_3RR activities of these electrodes, we quantified their ECSA, which is proportional to the double-layer capacitance. As demonstrated in Figure S8, the double-layer capacitance of the electrodes was measured using a CV method, and the capacitance increased from 1.32 mF for the Cu foam to 7.28 mF for the CuNW-15 electrode, confirming the creation of new catalytic sites for the NO_3RR on the Cu nanowire samples. Meanwhile, the capacitance only increased slightly to 7.88 mF for the CuNW-20 electrode, also explaining the little improvement of the NO_3RR catalytic performance from CuNW-15 to CuNW-20. As the CuNW-15 electrode showed a near-optimal performance for the NO_3RR to NH_3, it will be used as a representative Cu nanowire electrode for further studies below.

To understand the NO_3RR kinetics, we investigated the potential dependence of the NO_3RR performance on the Cu foam and CuNW-15 electrodes. They were evaluated by bulk electrolysis at selected potentials in 1 M KOH + 5 mM KNO_3 electrolyte. As the potential shifted from 0.1 to −0.3 V, the current density on the Cu foam increased almost exponentially from 0.8 to 24.4 mA cm^{-2}, while the current density on the CuNW-15 were generally higher, increasing rapidly from 1.4 to 33.1 mA cm^{-2}, as shown in Figure 4a. However, the increase of current density on the CuNW-15 was slower than the exponential trend at potentials <−0.1 V, due to the mass transport limitation. Meanwhile, the NH_3 Faradaic efficiency on CuNW-15 increased from 10.8% at 0.1 V to 90% at −0.1 V, and then dropped slightly to 86.3% at −0.3 V, which was accompanied by the emerging of the HER activity at the potential. In comparison, the NH_3 Faradaic efficiency on the Cu foam increased monotonically from 16.7% at 0.1 V to 50.1% at −0.1 V, and further to 82.8% at −0.3 V, which is generally lower than that on the CuNW-15 (Figure 4b). Consistently, the NO_2^- Faradaic efficiency decreased monotonically at more negative potentials on both electrodes. This relationship indicates a more favorable selectivity of NH_3 over NO_2^- at higher overpotentials. Compared to the Cu foam with a NH_3 Faradaic efficiency of 82.8% at −0.3 V, the CuNW-15 electrode achieved the highest NH_3 Faradaic efficiency of 90% at a lower overpotential (−0.1 V), confirming an enhanced activity and selectivity for the NO_3RR to NH_3 on the CuNW-15 electrode.

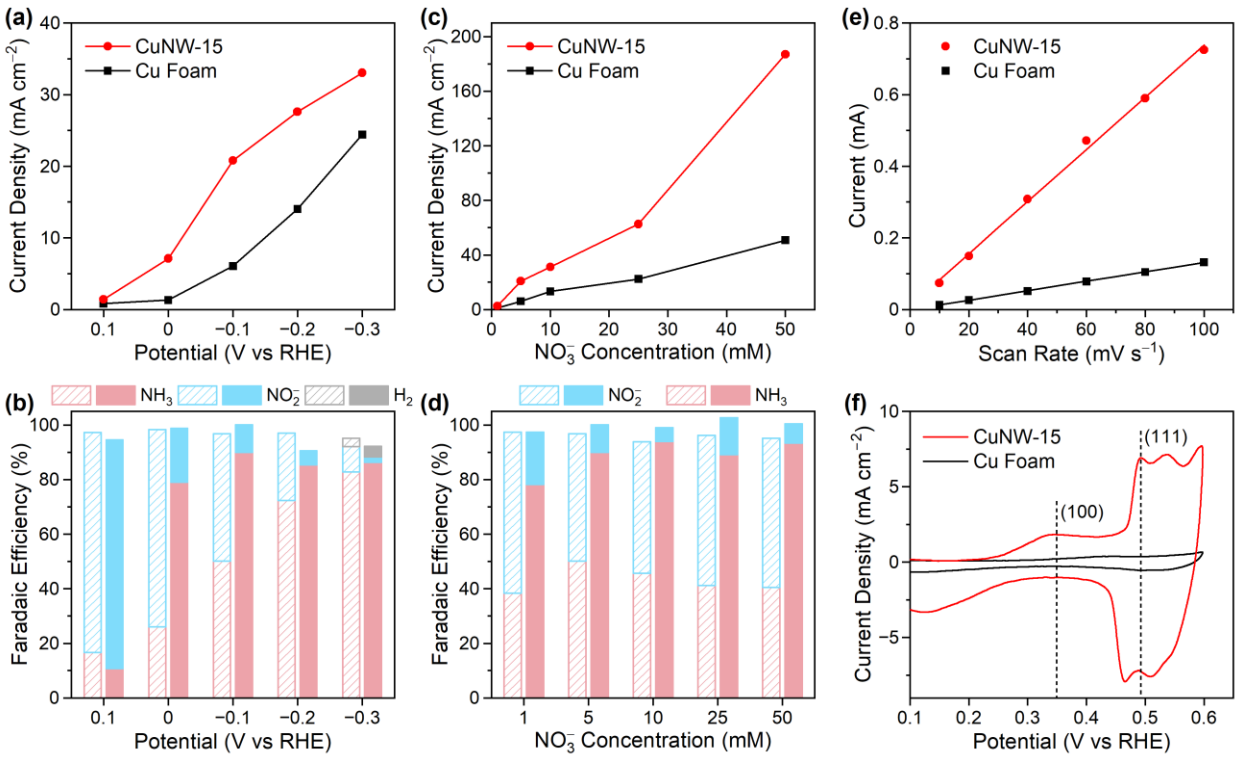

Figure 4. Comparison of the Cu foam and CuNW-15 electrodes for the NO_3RR in H-cell. (a) Total current densities and (b) Faradaic efficiencies for bulk electrolysis on the two electrodes at various potentials in 1 M KOH + 5 mM KNO_3 electrolyte. (c) Total current densities and (d) Faradaic efficiencies for bulk electrolysis on the two electrodes at −0.1 V vs RHE in 1 M KOH electrolytes containing different concentrations of NO_3^-. In (b) and (d), the left column with slash pattern at each value is for the Cu foam, and the right column with no pattern is for CuNW-15. (e) Double-layer charging current plotted against CV scan rate for the two electrodes. The slope of the linear regression gives the double-layer capacitance. (f) CV curves recorded on the two electrodes in Ar-saturated 1 M KOH electrolyte for the OH electrosorption tests. Scan rate: 100 mV s^{-1}.

As the NO_3^- concentration plays an important role in the NO_3RR kinetics,[42] the Cu foam and CuNW-15 electrodes were then evaluated for NO_3RR in 1 M KOH electrolytes containing various concentrations of NO_3^- at −0.1 V vs RHE. As shown in Figure 4c, the current density on the two electrodes both increased rapidly as the NO_3^- concentration increased from 1 to 50 mM, while the current densities on CuNW-15 were generally higher than those on the Cu foam in all electrolytes, further showing a substantial improvement of the NO_3RR activity due to a higher catalytic surface area of the CuNW-15 electrode, as will be discussed later. Interestingly, the increase of the current density with the NO_3^- concentration was faster than the linear trend, particularly in the case of 50 mM, so a higher NO_3^- concentration seemed more beneficial to the NO_3RR activity. In contrast, the NO_3RR selectivity showed a weak dependence on the NO_3^- concentration. As shown in Figure

4d, the CuNW-15 electrode showed Faradaic efficiencies of ~90% for NH_3 production and ~10% for NO_2^- production in most electrolytes. However, the Cu foam only showed Faradaic efficiencies of ~50% and ~50% for the production of NH_3 and NO_2^-, respectively. Therefore, the CuNW-15 electrode has a much higher intrinsic selectivity for the NO_3RR to NH_3, regardless of the NO_3^- concentration. Such a performance of the CuNW-15 electrode makes it a promising candidate for applications in the treatment of wastewater sources that have various concentrations of NO_3^-.[3,4]

To reveal the mechanisms underlying the enhanced activity and selectivity, the ECSA of the two electrodes was further compared. As shown in Figure 4e, the double-layer charging current was plotted against the CV scan rate for the two electrodes, and the slope of linear regression lines gave a double-layer capacitance of 1.32 and 7.28 mF for the Cu foam and CuNW-15 electrodes, respectively. Therefore, the ECSA of the CuNW-15 electrode is around 5.5 times that of the Cu foam, which directly contributed to the higher current density and NO_3RR activity.[43] However, this may not account for the large improvement of the NH_3 selectivity (Figure 4d) yet, so we further examined the surface structure and exposed facets of the two electrodes using the electrosorption of hydroxide.[28] As shown in Figure 4f, the CV curve recorded on the Cu foam showed no apparent features of surface facets, similar to that of Cu foil surface.[28] In contrast, the CuNW-15 sample exhibited a feature at around 0.35 V vs RHE corresponding to the Cu(100) facets, as well as an even higher peak for the Cu(111) facets. According to recent studies, while the Cu(100) surface is more active for the NO_3RR,[44] the NO_2^- generated on the Cu(100) facets can be subsequently reduced to NH_3 on the Cu(111) facets,[34] forming an efficient tandem electrocatalytic system for overall reduction of NO_3^- to NH_3. The CuNW-15 sample in our work showed an appropriate combination of exposed Cu(100) and Cu(111) facets, and thus significantly enhanced the intrinsic selectivity for NH_3 production. We also characterized the morphology of the CuNW-15 electrode after being tested for the NO_3RR, as shown by the SEM image in Figure S9, where the nanowire morphology remained largely similar with some minor surface changes.

The abovementioned studies have revealed the effect of Cu nanowire morphology and surface structure on the NO_3RR catalysis in H-cell, which provided a relatively simple testing environment of the NO_3RR. Considering the applications of the electrodes for wastewater treatment, we further developed a single-pass flow cell to simulate a flow system for the wastewater treatment and NO_3^- recycling to NH_3. A schematic diagram of the flow cell is shown in Figure 5a, with the CuNW-15 electrode and an Fe−Ni foam each inserted in a pocket of Ti current collector as the cathode and the anode, respectively.[45,46] A leak-free Ag/AgCl electrode was inserted in a 3D-printed chamber between the electrodes as the reference electrode.[45,46] The CuNW-15 and Cu foam electrodes were then evaluated for continuous NO_3^- reduction electrolysis using the flow cell with 1 M KOH + 5 mM KNO_3 electrolyte. Single-pass conversion tests were performed on the two electrodes at −0.1 V vs RHE, with the electrolyte passing through the foam electrodes at various flow rates, ranging from 15 to 60 mL h^{-1}.

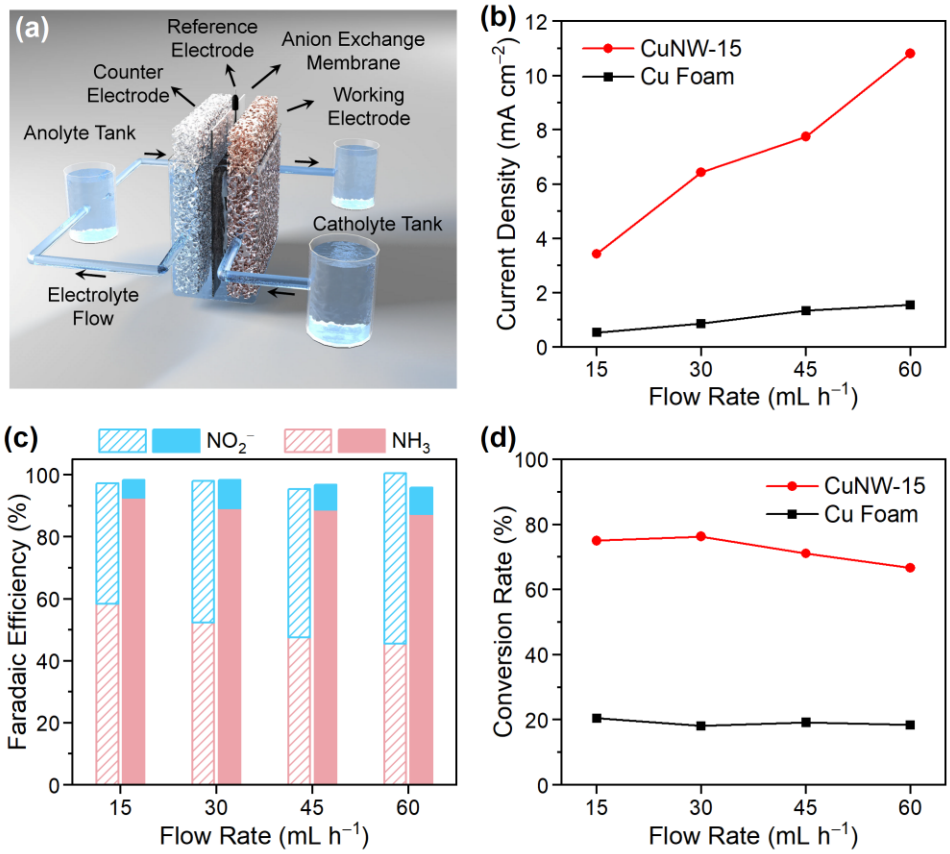

Figure 5. Evaluation of the NO_3RR performance on the Cu foam and CuNW-15 electrodes using single-pass flow cell. (a) Schematic illustration of the single-pass flow cell setup. (b) Total current densities, (c) Faradaic efficiencies, and (d) single-pass conversion rates for bulk electrolysis on the two electrodes at −0.1 V vs RHE under various electrolyte flow rates (1 M KOH + 5 mM KNO_3). In (c), the left column with slash pattern at each flow rate is for the Cu foam, and the right column with no pattern is for CuNW-15.

As shown in Figure 5b, the current density on both electrodes increased almost linearly with the increase of electrolyte flow rate, suggesting efficient interaction of NO_3^- with catalytic surfaces at elevated flow rates, benefiting from the porous foam structure. Specifically, as the electrolyte flow rate increased from 15 to 60 mL h^{-1}, the current density on the CuNW-15 electrode increased from 3.4 to 10.8 mA cm^{-2}, which is significantly higher than that on the Cu foam electrode, only rising from 0.53 to 1.55 mA cm^{-2}. Meanwhile, the highest NH_3 Faradaic efficiency of 92.6% was achieved on the CuNW-15 electrode at a flow rate of 15 mL h^{-1}, which only dropped slightly to 87.4% at a flow rate of 60 mL h^{-1}, as shown in Figure 5c. In contrast, the NH_3 Faradaic efficiency on the Cu foam ranged from 58.3% to 45.5% under the same conditions. Therefore, both NO_3RR activity and NH_3 selectivity were substantially improved on the CuNW-15 electrode compared to the Cu foam in the single-pass conversion tests. Moreover, the single-pass conversion rate of NO_3^-

in the electrolyte, defined as percentage of reactant converted per total reactant input, was derived as an important performance metric for practical applications. As shown in Figure 5d, the CuNW-15 electrode reached the highest single-pass conversion of 76.3% at the flow rate of 30 mL h^{-1}, which is 4.2 times that on the Cu foam under the same conditions, benefiting from the high activity and selectivity due to the high ECSA with an appropriate combination of exposed Cu(100) and Cu(111) facets. Overall, the CuNW-15 electrode, as a representative of the Cu nanowire electrodes, achieved a highly efficient process for single-pass NO_3^- recycling and NH_3 production from dilute NO_3^- solution, which can facilitate the development of efficient electrolyzers towards sustainable nitrogen-cycle transformations.

CONCLUSIONS

In summary, we have demonstrated a Cu nanowire electrocatalyst for efficient conversion of dilute NO_3^- to NH_3, which was prepared by growing Cu nanowires with tunable morphology and density on a Cu foam substrate. Compared to the Cu foam, the optimized Cu nanowire electrode (CuNW-15) showed greatly enhanced activity and selectivity for the NO_3RR to NH_3, achieving a current density of 20.8 mA cm^{-2} and a NH_3 Faradaic efficiency of 90% at a low overpotential of −0.1 V vs RHE in an H-cell with an electrolyte containing 5 mM NO_3^-. This is attributed to the high ECSA of the CuNW-15 electrode with an appropriate combination of Cu(100) and Cu(111) facets. The electrode was further evaluated for continuous NO_3^- recycling using a flow cell, which achieved a 76.3% single-pass conversion of dilute NO_3^- (5 mM) to NH_3 while maintaining a NH_3 Faradaic efficiency of 93%. Our work not only revealed structure-activity-selectivity relationships of the Cu nanowire electrocatalysts for NO_3^- reduction, but also demonstrated a promising method for NO_3^- recycling and NH_3 production from dilute NO_3^- solutions, towards sustainable nitrogen-cycle transformations.

ASSOCIATED CONTENT

Supporting Information

The Supporting Information is available free of charge at …

Additional experimental details, materials characterization, and electrochemical measurements (Figures S1−S9).

AUTHOR INFORMATION

ORCID: Kaige Shi: 0000-0003-1372-0210

Xiaofeng Feng: 0000-0002-9473-2848

Notes: The authors declare no competing financial interest.

ACKNOWLEDGMENTS

This material is based upon work supported by the National Science Foundation (NSF) under Grant No. 1943732. The authors acknowledge the use of an XPS instrument supported by the NSF MRI: ECCS: 1726636.

REFERENCES

(1) Zeng, Y.; Priest, C.; Wang, G.; Wu, G. Restoring the nitrogen cycle by electrochemical reduction of nitrate: progress and prospects. *Small Methods* **2020**, *4*, 2000672.

(2) Canfield, D. E.; Glazer, A. N.; Falkowski, P. G. The evolution and future of Earth's nitrogen cycle. *Science* **2010**, *330*, 192−196.

(3) Ascott, M. J.; Gooddy, D. C.; Wang, L.; Stuart, M. E.; Lewis, M. A.; Ward, R. S.; Binley, A. M. Global patterns of nitrate storage in the vadose zone. *Nat. Commun.* **2017**, *8*, 1416.

(4) Choudhary, M.; Muduli, M.; Ray, S. A comprehensive review on nitrate pollution and its remediation: conventional and recent approaches. *Sustain. Water Resour. Manag.* **2022**, *8*, 113.

(5) Fernandez, C. A.; Hortance, N. M.; Liu, Y. H.; Lim, J.; Hatzell, K. B.; Hatzell, M. C. Opportunities for intermediate temperature renewable ammonia electrosynthesis. *J. Mater. Chem. A* **2020**, *8*, 15591−15606.

(6) Hu, L.; Pillai, H. S.; Feit, C.; Shi, K.; Gao, Z.; Banerjee, P.; Xin, H.; Feng, X. Identification of active sites for ammonia electrosynthesis on ruthenium. *ACS Energy Lett.* **2022**, *7*, 4290−4298.

(7) van Langevelde, P. H.; Katsounaros, I.; Koper, M. T. Electrocatalytic nitrate reduction for sustainable ammonia production. *Joule* **2021**, *5*, 290−294.

(8) Wang, Y.; Wang, C.; Li, M.; Yu, Y.; Zhang, B. Nitrate electroreduction: mechanism insight, in situ characterization, performance evaluation, and challenges. *Chem. Soc. Rev.* **2021**, *50*, 6720−6733.

(9) Zhang, X.; Wang, Y.; Liu, C.; Yu, Y.; Lu, S.; Zhang, B. Recent advances in non-noble metal electrocatalysts for nitrate reduction. *Chem. Eng. J.* **2021**, *403*, 126269.

(10) Liang, X.; Zhu, H.; Yang, X.; Xue, S.; Liang, Z.; Ren, X.; Liu, A.; Wu, G. Recent advances in designing efficient electrocatalysts for electrochemical nitrate reduction to ammonia. *Small Struct.* **2023**, *4*, 2200202.

(11) Jia, R.; Wang, Y.; Wang, C.; Ling, Y.; Yu, Y.; Zhang, B. Boosting selective nitrate electroreduction to ammonium by constructing oxygen vacancies in TiO_2. *ACS Catal.* **2020**, *10*, 3533−3540.
(12) Wu, Z. Y.; Karamad, M.; Yong, X.; Huang, Q.; Cullen, D. A.; Zhu, P.; Xia, C.; Xiao, Q.; Shakouri, M.; Chen, F. Y.; et al. Electrochemical ammonia synthesis via nitrate reduction on Fe single atom catalyst. *Nat. Commun.* **2021**, *12*, 2870.
(13) Lim, J.; Liu, C. Y.; Park, J.; Liu, Y. H.; Senftle, T. P.; Lee, S. W.; Hatzell, M. C. Structure sensitivity of Pd facets for enhanced electrochemical nitrate reduction to ammonia. *ACS Catal.* **2021**, *11*, 7568−7577.
(14) Jeon, T. H.; Wu, Z. Y.; Chen, F. Y.; Choi, W.; Alvarez, P. J.; Wang, H. Cobalt–copper nanoparticles on three-dimensional substrate for efficient ammonia synthesis via electrocatalytic nitrate reduction. *J. Phys. Chem. C* **2022**, *126*, 6982−6989.
(15) He, W.; Zhang, J.; Dieckhöfer, S.; Varhade, S.; Brix, A. C.; Lielpetere, A.; Seisel, S.; Junqueira, J. R. C.; Schuhmann, W. Splicing the active phases of copper/cobalt-based catalysts achieves high-rate tandem electroreduction of nitrate to ammonia. *Nat. Commun.* **2022**, *13*, 1129.
(16) Gao, Q.; Pillai, H. S.; Huang, Y.; Liu, S.; Mu, Q.; Han, X.; Yan, Z.; Zhou, H.; He, Q.; Xin, H.; et al. Breaking adsorption-energy scaling limitations of electrocatalytic nitrate reduction on intermetallic CuPd nanocubes by machine-learned insights. *Nat. Commun.* **2022**, *13*, 338.
(17) Harmon, N. J.; Rooney, C. L.; Tao, Z.; Shang, B.; Raychaudhuri, N.; Choi, C.; Li, H.; Wang, H. Intrinsic catalytic activity of carbon nanotubes for electrochemical nitrate reduction. *ACS Catal.* **2022**, *12*, 9135−9142.
(18) Gao, Q.; Yao, B.; Pillai, H. S.; Zang, W.; Han, X.; Liu, Y.; Yu, S. W.; Yan, Z.; Min, B.; Zhang, S.; et al. Synthesis of core/shell nanocrystals with ordered intermetallic single-atom alloy layers for nitrate electroreduction to ammonia. *Nat. Synth.* **2023**, *2*, 624−634.
(19) Han, S.; Li, H.; Li, T.; Chen, F.; Yang, R.; Yu, Y.; Zhang, B. Ultralow overpotential nitrate reduction to ammonia via a three-step relay mechanism. *Nat. Catal.* **2023**, *6*, 402−414.
(20) Li, B.; Xia, F.; Liu, Y.; Tan, H.; Gao, S.; Kaelin, J.; Liu, Y.; Lu, K.; Marks, T. J.; Cheng, Y. $Co_2Mo_6S_8$ catalyzes nearly exclusive electrochemical nitrate conversion to ammonia with enzyme-like activity. *Nano Lett.* **2023**, *23*, 1459−1466.
(21) Wang, X.; Wu, X.; Ma, W.; Zhou, X.; Zhang, S.; Huang, D.; Winter, L. R.; Kim, J. H.; Elimelech, M. Free-standing membrane incorporating single-atom catalysts for ultrafast electroreduction of low-concentration nitrate. *Proc. Natl. Acad. Sci. U.S.A.* **2023**, *120*, e2217703120.
(22) Hu, T.; Wang, C.; Wang, M.; Li, C. M.; Guo, C. Theoretical insights into superior nitrate reduction to ammonia performance of copper catalysts. *ACS Catal.* **2021**, *11*, 14417−14427.

(23) Reyter, D.; Chamoulaud, G.; Bélanger, D.; Roué, L. Electrocatalytic reduction of nitrate on copper electrodes prepared by high-energy ball milling. *J. Electroanal. Chem.* **2006**, *596*, 13−24.
(24) Reyter, D.; Bélanger, D.; Roué, L. Study of the electroreduction of nitrate on copper in alkaline solution. *Electrochim. Acta* **2008**, *53*, 5977−5984.
(25) Abdallah, R.; Geneste, F.; Labasque, T.; Djelal, H.; Fourcade, F.; Amrane, A.; Taha, S.; Floner, D. Selective and quantitative nitrate electroreduction to ammonium using a porous copper electrode in an electrochemical flow cell. *J. Electroanal. Chem.* **2014**, *727*, 148−153.
(26) Mattarozzi, L.; Cattarin, S.; Comisso, N.; Gambirasi, A.; Guerriero, P.; Musiani, M.; Vázquez-Gómez, L.; Verlato, E. Hydrogen evolution assisted electrodeposition of porous Cu-Ni alloy electrodes and their use for nitrate reduction in alkali. *Electrochim. Acta* **2014**, *140*, 337−344.
(27) Butcher Jr, D. P.; Gewirth, A. A. Nitrate reduction pathways on Cu single crystal surfaces: Effect of oxide and Cl^-. *Nano Energy* **2016**, *29*, 457−465.
(28) Fu, X.; Zhao, X.; Hu, X.; He, K.; Yu, Y.; Li, T.; Tu, Q.; Qian, X.; Yue, Q.; Wasielewski, M. R.; et al. Alternative route for electrochemical ammonia synthesis by reduction of nitrate on copper nanosheets. *Appl. Mater. Today* **2020**, *19*, 100620.
(29) Wang, Y.; Zhou, W.; Jia, R.; Yu, Y.; Zhang, B. Unveiling the activity origin of a copper-based electrocatalyst for selective nitrate reduction to ammonia. *Angew. Chem. Int. Ed.* **2020**, *59*, 5350−5354.
(30) Yuan, J.; Xing, Z.; Tang, Y.; Liu, C. Tuning the oxidation state of Cu electrodes for selective electrosynthesis of ammonia from nitrate. *ACS Appl. Mater. Interfaces* **2021**, *13*, 52469−52478.
(31) Wang, Y.; Qin, X.; Shao, M. First-principles mechanistic study on nitrate reduction reactions on copper surfaces: Effects of crystal facets and pH. *J. Catal.* **2021**, *400*, 62−70.
(32) Chen, F. Y.; Wu, Z. Y.; Gupta, S.; Rivera, D. J.; Lambeets, S. V.; Pecaut, S.; Kim, J. Y. T.; Zhu, P.; Finfrock, Y. Z.; Meira, D. M.; et al. Efficient conversion of low-concentration nitrate sources into ammonia on a Ru-dispersed Cu nanowire electrocatalyst. *Nat. Nanotechnol.* **2022**, *17*, 759−767.
(33) Zhou, N.; Wang, Z.; Zhang, N.; Bao, D.; Zhong, H.; Zhang, X. Potential-induced synthesis and structural identification of oxide-derived Cu electrocatalysts for selective nitrate reduction to ammonia. *ACS Catal.* **2023**, *13*, 7529−7537.
(34) Fu, Y.; Wang, S.; Wang, Y.; Wei, P.; Shao, J.; Liu, T.; Wang, G.; Bao, X. Enhancing electrochemical nitrate reduction to ammonia over Cu nanosheets via facet tandem catalysis. *Angew. Chem. Int. Ed.* **2023**, *62*, e202303327.

(35) Chen, J. Q.; Ye, X. X.; Zhou, D.; Chen, Y. X. Roles of copper in nitrate reduction at copper-modified Ru/C catalysts. *J. Phys. Chem. C* **2023**, *127*, 2918−2928.
(36) Zhang, W.; Wen, X.; Yang, S.; Berta, Y.; Wang, Z. L. Single-crystalline scroll-type nanotube arrays of copper hydroxide synthesized at room temperature. *Adv. Mater.* **2003**, *15*, 822−825.
(37) Ma, M.; Djanashvili, K.; Smith, W. A. Selective electrochemical reduction of CO_2 to CO on CuO-derived Cu nanowires. *Phys. Chem. Chem. Phys.* **2015**, 17, 20861−20867.
(38) Searle, P. L. The Berthelot or indophenol reaction and its use in the analytical chemistry of nitrogen. *Analyst* **1984**, *109*, 549−568.
(39) Green, L. C.; Wagner, D. A.; Glogowski, J.; Skipper, P. L.; Wishnok, J. S.; Tannenbaum, S. R. Analysis of nitrate, nitrite, and [^{15}N] nitrate in biological fluids. *Anal. Biochem.* **1982**, *126*, 131−138.
(40) Larson, P. E. X-ray induced photoelectron and auger spectra of Cu, CuO, Cu_2O, and Cu_2S thin films. *J. Electron Spectrosc. Relat. Phenom.* **1974**, *4*, 213−218.
(41) Platzman, I.; Brener, R.; Haick, H.; Tannenbaum, R. Oxidation of polycrystalline copper thin films at ambient conditions. *J. Phys. Chem. C* **2008**, *112*, 1101−1108.
(42) Barrera, L.; Silcox, R.; Giammalvo, K.; Brower, E.; Isip, E.; Bala Chandran, R. Combined effects of concentration, pH, and polycrystalline copper surfaces on electrocatalytic nitrate-to-ammonia activity and selectivity. *ACS Catal.* **2023**, *13*, 4178−4192.
(43) Ren, Z.; Shi, K.; Feng, X. Elucidating the intrinsic activity and selectivity of Cu for nitrate electroreduction. *ACS Energy Lett.* **2023**, *8*, 3658−3665.
(44) Pérez-Gallent, E.; Figueiredo, M. C.; Katsounaros, I.; Koper, M. T. M. Electrocatalytic reduction of Nitrate on Copper single crystals in acidic and alkaline solutions. *Electrochim. Acta* **2017**, *227*, 77−84.
(45) Xing, Z.; Hu, L,; Ripatti, D. S.; Hu, X.; Feng, X. Enhancing carbon dioxide gas-diffusion electrolysis by creating a hydrophobic catalyst microenvironment. *Nat. Commun.* **2021**, *12*, 136.
(46) Xing, Z.; Hu, X.; Feng, X. Tuning the microenvironment in gas-diffusion electrodes enables high-rate CO_2 electrolysis to formate. *ACS Energy Lett.* **2021**, *6*, 1694−1702.

TOC Graphic:

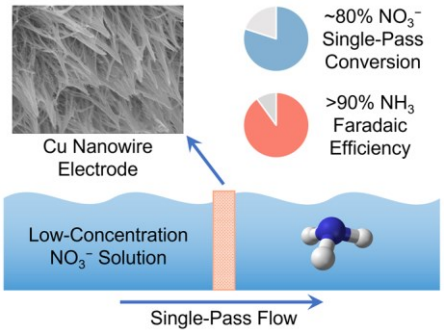
~80% NO_3^- Single-Pass Conversion
>90% NH_3 Faradaic Efficiency
Cu Nanowire Electrode
Low-Concentration NO_3^- Solution
Single-Pass Flow